



## THERMODYNAMIC AND STRUCTURAL PROPERTIES OF BIOMIMETIC MONOLAYERS CONTAINING CHOLESTEROL AND MAGNETITE NANOPARTICLES

Nagihan SOYER<sup>1\*</sup>, Sema SALGIN<sup>1</sup>, Uğur SALGIN<sup>1</sup>

<sup>1</sup>Sivas Cumhuriyet University, Faculty of Engineering, Department of Chemical Engineering, 58140, Sivas, Türkiye

**Abstract:** The thermodynamic and structural properties of biomimetic monolayers composed of cholesterol, dipalmitoylphosphatidylcholine, and hydrophobic magnetite ( $\text{Fe}_3\text{O}_4$ ) nanoparticles were investigated under varying cholesterol molar fractions and pH conditions (4.8 and 7.4). Langmuir monolayer experiments were performed to analyze surface pressure-area isotherms, excess molecular area, excess Gibbs free energy of mixing, and compressibility modulus to assess lipid monolayer phase behavior, molecular organization, and mechanical stability. The results confirm that cholesterol enhances monolayer condensation up to a cholesterol molar fraction of 0.50, particularly at pH 7.4, where stronger lipid-lipid interactions promote molecular ordering and increase monolayer rigidity. At cholesterol molar fractions of 0.75 and higher, steric hindrance and phase separation effects emerge, disrupting monolayer homogeneity. pH significantly influences monolayer stability, with pH 7.4 favoring lipid condensation, whereas pH 4.8 induces monolayer expansion and molecular disorder. Excess molecular area and Gibbs free energy of mixing analyses indicate the strongest cholesterol-lipid interactions at a cholesterol molar fraction of 0.25 for pH 4.8 and 0.50 for pH 7.4, confirming these compositions as the most thermodynamically stable. Compressibility modulus analysis demonstrates that cholesterol enhances monolayer rigidity, with pH 7.4 producing higher values. However, at high cholesterol molar fractions, compressibility modulus slightly decrease, suggesting steric constraints and lateral phase separation. The incorporation of magnetite nanoparticles increases molecular area and slightly reduces monolayer rigidity at low cholesterol molar fractions due to steric disruptions, but at cholesterol molar fractions of 0.50 and higher, cholesterol stabilizes the monolayer, counteracting nanoparticle-induced perturbations. These findings provide insight into the thermodynamic and structural regulation of biomimetic lipid monolayers by cholesterol and magnetite nanoparticles, with implications for nanomedicine, membrane biophysics, and lipid-based nanostructures.

**Keywords:** Cholesterol, Dipalmitoylphosphatidylcholine, Hydrophobic Magnetite nanoparticles, Monolayer stability, Surface pressure, Phase behavior

\*Corresponding author: Sivas Cumhuriyet University, Faculty of Engineering, Department of Chemical Engineering, 58140, Sivas, Türkiye

E mail: nsoyer@cumhuriyet.edu.tr (N. SOYER)

Nagihan SOYER  <https://orcid.org/0000-0003-1342-2037>

Sema SALGIN  <https://orcid.org/0000-0001-6354-3553>

Uğur SALGIN  <https://orcid.org/0000-0002-5683-7569>

Received: March 05, 2025

Accepted: April 09, 2025

Published: May 15, 2025

**Cite as:** Soyer N, Salgin S, Salgin U. 2025. Thermodynamic and structural properties of biomimetic monolayers containing cholesterol and magnetite nanoparticles. *BSJ Eng Sci*, 8(3): 837-845.

### 1. Introduction

Cell membranes play a fundamental role in regulating biological processes, including molecular transport, signal transduction, and structural organization. Their biophysical properties are largely governed by the interplay between lipid composition, phase behavior, and environmental conditions (Jurak et al., 2018). Among the key lipid components, dipalmitoylphosphatidylcholine (DPPC), a major phospholipid in cell membranes and pulmonary surfactants, is well known for its thermotropic phase transitions, shifting between gel, liquid-expanded (LE), and liquid-condensed (LC) phases depending on temperature and molecular interactions (Ding et al., 2016; Zhang et al., 2016). Cholesterol (Chol), another critical membrane component, interacts with phospholipids to modulate bilayer rigidity, lipid domain formation, and phase stability (Rosilio, 2017). The specific interactions between Chol and DPPC significantly affect membrane permeability and mechanical

properties, making this system a widely used model in biomembrane research (Oliveira et al., 2022). To investigate the phase behavior of lipid assemblies under controlled conditions, Langmuir monolayers have emerged as a powerful model system. These monolayers allow for precise control over lipid composition, surface pressure ( $\pi$ ), and molecular organization, thereby enabling systematic studies of lipid-lipid and lipid-nanoparticle interactions (Moya Betancourt et al., 2023; Swierczewski and Bürgi, 2023). The incorporation of nanoparticles (NPs) into biomimetic membranes has drawn increasing interest due to their applications in biosensing, targeted drug delivery, and nanomedicine (Piosik et al., 2021; Peetla et al., 2014). Magnetic  $\text{Fe}_3\text{O}_4$  nanoparticles (MNPs) are promising candidates in biomedicine due to their superparamagnetic properties, biocompatibility, and surface functionalization potential (Hao et al., 2016; Salas et al., 2024). Previous studies suggest that MNPs alter lipid monolayer structure,



leading to changes in lipid packing, phase behavior, and membrane elasticity, but the combined effects of cholesterol, pH, and MNPs remain underexplored (Rosilio, 2017). Recent research has demonstrated that pH plays a crucial role in determining lipid monolayer stability and molecular organization. Under acidic conditions (pH 4.8), intermolecular interactions between DPPC molecules are strengthened, leading to higher packing densities and lower molecular mobility (Ding et al., 2016; Zhang et al., 2016). Conversely, neutral pH (pH 7.4) promotes a more fluid monolayer structure, reducing lipid-lipid interactions and favoring molecular expansion (Cullis et al., 1997). These pH-dependent behaviors are particularly relevant in biological systems, where lipid membranes are exposed to varying pH environments, such as extracellular fluids (pH ~7.4) and endosomal compartments (pH ~4.8 - 5.5) (He et al., 2014). Additionally, pH-driven alterations in lipid monolayers influence nanoparticle adsorption, Chol miscibility, and lipid domain formation, further highlighting the need for systematic investigations (Rosilio, 2017). This study aims to systematically investigate the interdependent effects of  $x_{\text{Chol}}$ , pH, and  $\text{Fe}_3\text{O}_4$  MNPs on lipid monolayer phase behavior, thermodynamic properties, and mechanical stability. Surface pressure-area isotherms, excess molecular area, excess Gibbs free energy of mixing, and compressibility modulus were analyzed to quantify these effects across varying  $x_{\text{Chol}}$  and pH conditions. By providing a comprehensive assessment of these parameters, this research advances our understanding of lipid-nanoparticle interactions, biomimetic membrane stability, and nanostructured lipid platforms for drug delivery applications.

## 2. Materials and Methods

### 2.1. Materials

The biomimetic membrane model components, including DPPC and Chol, were purchased from Avanti Polar Lipids Inc. (USA). Hydrophobic  $\text{Fe}_3\text{O}_4$  MNPs ( $\leq 5$  nm), anhydrous chloroform, anhydrous methanol, and sodium phosphate salts were obtained from Sigma-Aldrich (Germany). Ultrapure water (conductivity: 18.2 M $\Omega$  cm) from a Milli-Q system (Millipore) was used for solution preparation and the cleaning of the Langmuir-Blodgett (LB) trough, ensuring contaminant removal and maintaining experimental precision.

### 2.2. Langmuir Monolayer Experiments

Chol/DPPC-MNP monolayers were prepared using a Langmuir-Blodgett trough (KSV NIMA 2000, KSV Instruments Ltd., Helsinki, Finland) with a surface area of 273 cm<sup>2</sup>. The system was equipped with movable Delrin barriers, a Wilhelmy plate for surface pressure measurements, and an electronic balance with a resolution of 4  $\mu\text{N/m}$ . The trough and barriers were made of Teflon, ensuring chemical resistance and minimal contamination.

The surface pressure ( $\pi$ ) was measured using the Wilhelmy plate method and was calculated according to equation 1:

$$\pi = \gamma_0 - \gamma \quad (1)$$

where  $\gamma_0$  represents the surface tension of the subphase in the absence of a monolayer, and  $\gamma$  corresponds to the surface tension measured when the monolayer is present (Wrobel et al., 2024; Szcześ et al., 2012).

Prior to each experiment, the main components of the system, including the trough and Teflon barriers, were thoroughly cleaned with chloroform, methanol, and ultrapure water to eliminate contaminants. The subphase for Chol/DPPC-MNP monolayers consisted of 176 mL sodium phosphate buffer solutions at pH 4.8 and 7.4 to evaluate the impact of pH on lipid-nanoparticle interactions. The compression isotherms were obtained at a controlled temperature of  $24 \pm 0.1^\circ\text{C}$  using a refrigerated circulator (Haake C25P Phoenix II, ThermoElectron Co., USA) to ensure stable monolayer conditions. Surface pressure-area ( $\pi$ -A) isotherms were recorded to investigate the interaction of  $\text{Fe}_3\text{O}_4$  magnetic nanoparticles with phospholipid monolayers, simulating biomimetic membrane behavior. The Chol/DPPC-MNP stock solutions (1 mg/mL) were prepared in anhydrous chloroform at varying chol mole fractions ( $x_{\text{Chol}}=0, 0.25, 0.5, 0.75, \text{ and } 1.0$ ). For each experiment, 25  $\mu\text{L}$  of the solution was spread onto the subphase surface using a Hamilton micro syringe. The system was allowed to equilibrate for 15 minutes to ensure complete solvent evaporation. All isotherms were obtained under symmetric compression of the monolayers at a constant barrier speed of 5 mm/min, with measurements recorded automatically. Each experiment was performed in triplicate to ensure reproducibility.

### 2.3. Calculation of Thermodynamic and Structural Parameter

#### Mean Molecular Area ( $A_{12}$ )

The mean molecular area,  $A_{12}$ , was determined from  $\pi$ -A isotherms using equation 2:

$$A_{12} = \frac{A_{\text{measured}}}{N} \quad (2)$$

where  $A_{12}$  represents the mean molecular area ( $\text{\AA}^2/\text{molecule}$ ),  $A_{\text{measured}}$  is the total monolayer area at a given surface pressure ( $\text{\AA}^2$ ), and  $N$  is the number of lipid molecules at the interface.

#### Excess Molecular Area ( $A_{\text{exc}}$ )

The excess molecular area, which quantifies deviations from ideal mixing, was calculated using equation 3:

$$A_{\text{exc}} = A_{12}^{\text{real}} - A_{12}^{\text{ideal}} \quad (3)$$

where  $A_{12}^{\text{real}}$  is the experimentally measured molecular area, and  $A_{12}^{\text{ideal}}$  is the theoretical molecular area assuming ideal mixing, determined by equation 4:

$$A_{12}^{\text{ideal}} = x_1 A_1 + x_2 A_2 \quad (4)$$

Here,  $x_1$  and  $x_2$  are the mole fractions of lipid

components, and  $A_1$  and  $A_2$  are their respective molecular areas in pure form.

#### Excess Gibbs Free Energy of Mixing ( $\Delta G_{exc}$ )

The thermodynamic stability of the monolayer was assessed using the excess Gibbs free energy of mixing,  $\Delta G_{exc}$ , given by equation 5:

$$\Delta G_{exc} = N_A \int_0^\pi A_{exc} d\pi \quad (5)$$

where  $\Delta G_{exc}$  (J/mol) represents the excess free energy of mixing,  $N_A$  is Avogadro's number,  $A_{exc}$  is the excess molecular area, and  $\pi$  is the surface pressure (mN/m). Negative values of  $\Delta G_{exc}$  indicate favorable lipid-Chol interactions, while positive values suggest phase separation.

#### Compressibility Modulus ( $C_s^{-1}$ )

The compressibility modulus,  $C_s^{-1}$ , which describes the elasticity of the monolayer, was determined from the  $\pi$ -A isotherm using equation 6:

$$C_s^{-1} = -A \left( \frac{\partial \pi}{\partial A} \right)_T \quad (6)$$

where  $C_s^{-1}$  (mN/m) represents the compressibility modulus,  $A$  is the molecular area ( $\text{\AA}^2/\text{molecule}$ ), and  $(d\pi/dA)_T$  is the derivative of surface pressure with respect to molecular area at constant temperature. Higher  $C_s^{-1}$  values indicate a more rigid monolayer, while lower values correspond to a more fluid monolayer.

## 3. Results and Discussion

### 3.1. Surface Pressure-Area Isotherms

The  $\pi$ -A isotherms provide critical insights into the phase behavior, molecular organization, and thermodynamic stability of Chol/DPPC monolayers incorporating hydrophobic MNPs. The isotherms were recorded at varying  $x_{\text{Chol}}$  (0, 0.25, 0.5, 0.75, and 1.0) and pH conditions (4.8 and 7.4), allowing for the evaluation of how Chol and pH modulate lipid packing and phase transitions in the presence of MNPs (Moya Betancourt et al., 2023; Szcześ et al., 2012). The  $\pi$  was determined experimentally using the Wilhelmy plate method and calculated using equation 1. This equation was used to compute the real-time variations in  $\pi$  during monolayer compression, generating the  $\pi$ -A isotherms that describe the monolayer's phase behavior under different Chol and pH conditions. As shown in Figure 1, at low  $x_{\text{Chol}}$  ( $\leq 0.25$ ), the isotherms exhibit a LE to LC phase transition plateau between  $\sim 10$ -12 mN/m, indicating the coexistence of different molecular packing states within the monolayer. However, as  $x_{\text{Chol}}$  increases, the LE-LC transition gradually disappears, and the isotherms shift to smaller molecular areas, suggesting that Chol promotes lipid condensation and enhances molecular ordering (Cullis et al., 1997; Rosilio, 2017). At higher cholesterol concentrations ( $x_{\text{Chol}} \geq 0.5$ ), the phase transition plateaus disappear entirely, leading to a more homogeneous and rigid monolayer structure. The collapse pressure ( $\pi_a$ ), which defines the maximum surface pressure before

monolayer failure, increases from  $\sim 42$  mN/m at  $x_{\text{Chol}}=0$  to  $\sim 55$  mN/m at  $x_{\text{Chol}}=1.0$ , confirming the stabilizing effect of Chol in the presence of MNPs (Moya Betancourt et al., 2023; Ganta et al., 2008).

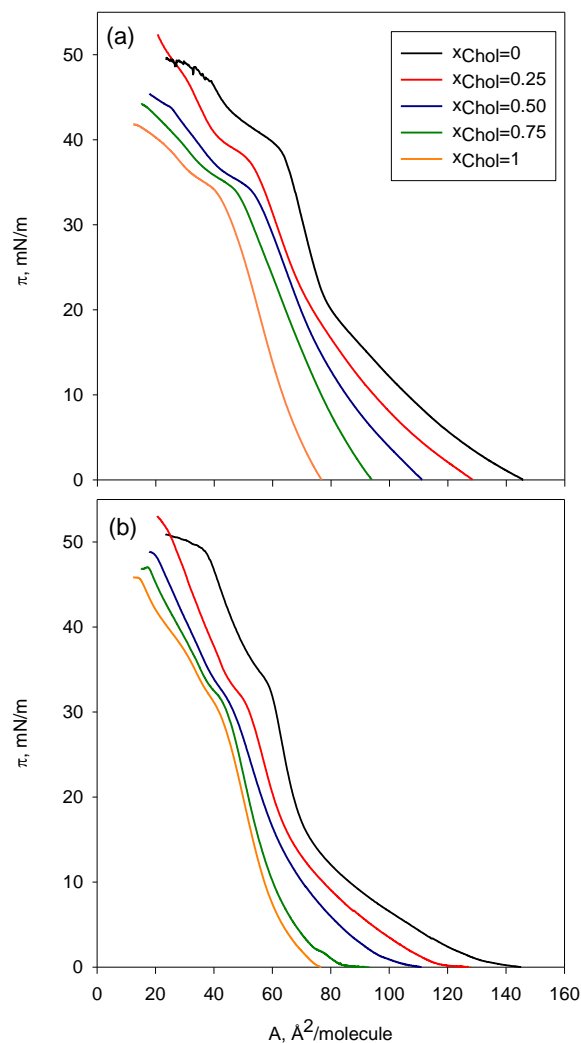


**Figure 1.**  $\pi$ -A isotherms obtained at different composition ratios of Chol/DPPC-MNP at (a) pH=4.8 and (b) pH=7.4.

The pH-dependent effects on monolayer behavior are evident in Figure 1, where monolayers at pH 4.8 (Figure 1a) exhibit larger molecular areas at a given  $\pi$  compared to pH 7.4 (Figure 1b), suggesting that acidic conditions weaken lipid-lipid interactions and reduce lipid packing efficiency. This expansion can be attributed to the protonation of DPPC phosphate headgroups at pH 4.8, which reduces electrostatic interactions, increasing intermolecular repulsion and promoting molecular disorder. As a result, Chol-lipid interactions are less pronounced under acidic conditions, leading to a more expanded monolayer structure (Ding et al., 2016; Gong et al., 2002). This effect is particularly pronounced at high  $x_{\text{Chol}}$  ( $\geq 0.5$ ), where the molecular area at  $\pi=30$  mN/m is  $\sim 40$   $\text{\AA}^2/\text{molecule}$  at pH 7.4, compared to  $\sim 55$   $\text{\AA}^2/\text{molecule}$  at pH 4.8, confirming that Chol integrates more efficiently into the monolayer at neutral pH. Figure

1 further confirms that the collapse pressure at pH 7.4 is consistently higher ( $\sim 5\text{-}8$  mN/m) than at pH 4.8, supporting the idea that pH modulates monolayer stability by altering lipid headgroup interactions. These findings align with previous studies, such as Gao et al. (2010), which highlight the role of pH-responsive nanoparticles in altering surface charge and molecular organization. Specifically, at lower pH levels, nanoparticles undergo swelling or charge modification, which may further influence monolayer expansion and disrupt lipid packing. This suggests that the observed increase in molecular area at acidic pH could be partially attributed to pH-dependent NP structural changes rather than solely lipid headgroup protonation. Since MNPs were incorporated in all experimental conditions, their effects must be evaluated alongside Chol and pH effects rather than as an independent variable. The presence of MNPs results in an overall monolayer expansion, as evidenced by the increased molecular area at a given  $\pi$  compared to Chol-DPPC systems without nanoparticles. Previous research (Bodik et al., 2020) indicates that the organization of nanomaterials within Langmuir monolayers is highly dependent on pH-controlled surface potential changes. However, at  $x_{\text{Chol}} \geq 0.5$ , the stabilizing effect of Chol counteracts this expansion, limiting MNP-induced disruptions in monolayer packing (Oliveira et al., 2022; Piosik et al., 2021). Moreover, the Langmuir monolayer stability is further confirmed by the collapse pressure values obtained for all Chol molar fractions. As shown in Figure 1, a single collapse pressure value is observed across all compositions, which, as noted by Jurak et al. (2018), indicates that the monolayer components are miscible. This suggests that Chol, DPPC, and MNPs form a stable monolayer structure without phase separation at all studied concentrations. Additionally, the absence of collapse up to approximately 46-48 mN/m surface pressure further confirms the successful formation of the Langmuir monolayers. This effect is particularly evident at pH 7.4, where enhanced lipid-lipid and lipid-Chol interactions contribute to monolayer stability.

### 3.2. Molecular Area Reduction and Lipid Mixing Behavior

The  $A_{12}\text{-}x_{\text{Chol}}$  analysis provides insight into how Chol influences the packing behavior of DPPC monolayers incorporating MNPs under different  $\pi$  and pH conditions (4.8 and 7.4) (Figure 2). This analysis helps determine whether Chol acts as a condensing agent by reducing  $A_{12}$  or whether it disrupts lipid organization at different compositions. The  $A_{12}$  values were determined experimentally from  $\pi\text{-}A$  isotherms and plotted as a function of  $x_{\text{Chol}}$ . The theoretical molecular area for an ideal mixture was calculated using equation 4), where component 1 (DPPC) and component 2 (Chol) denote the molar fractions and their respective molecular areas in pure monolayers. As shown in Figure 2,  $A_{12}$  values decrease progressively with increasing  $x_{\text{Chol}}$ , indicating that Chol enhances molecular condensation and lipid

ordering (Moya Betancourt et al., 2023; Szcześ et al., 2012). Figure 2(a) illustrates that at pH 4.8,  $A_{12}$  values remain consistently larger compared to Figure 2(b) at pH 7.4, supporting the idea that acidic conditions weaken lipid-lipid interactions and promote a more expanded monolayer (Ding et al., 2016; Gong et al., 2002). In contrast, at pH 7.4, stronger Chol-lipid interactions result in a more condensed lipid organization.

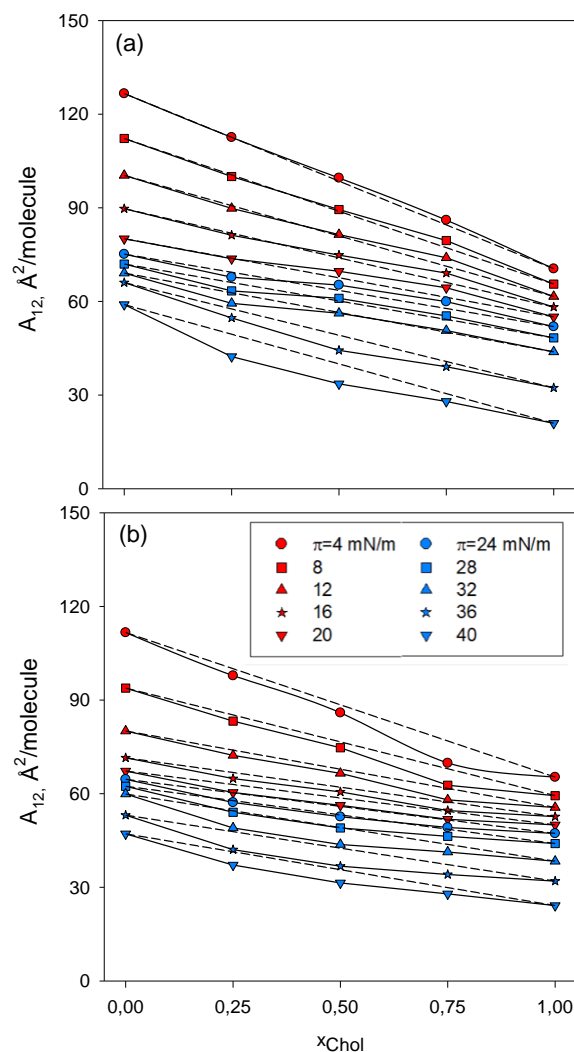


**Figure 2.**  $A_{12}\text{-}x_{\text{Chol}}$  curves obtained at different surface pressures for Chol/DPPC-MNP monolayers at (a) pH=4.8 and (b) pH=7.4.

A theoretical ideal mixture would exhibit a linear  $A_{12}\text{-}x_{\text{Chol}}$  curve, which indicates that the individual monolayer components do not interact and are not miscible (Dana, 1999). However, experimental  $A_{12}\text{-}x_{\text{Chol}}$  values deviate from this linear behavior, demonstrating that Chol, DPPC, and MNPs are interacting and forming a stable mixed monolayer. As shown in Figure 2, the experimental and theoretical  $A_{12}\text{-}x_{\text{Chol}}$  curves do not overlap, which is a direct result of intercomponent interactions and confirms the miscibility of Chol/DPPC-MNP monolayers. This deviation from ideality indicates that Chol and MNPs influence lipid organization, reinforcing lipid-lipid

interactions at specific compositions. The data indicates that at low  $x_{\text{Chol}}$  ( $\leq 0.25$ ), the  $A_{12}$  decreases gradually, suggesting that Chol is integrating into the monolayer while still allowing some lipid-lipid spacing. However, at  $x_{\text{Chol}} \geq 0.5$ ,  $A_{12}$  decreases more sharply, confirming that Chol enhances molecular condensation and promotes a more tightly packed lipid organization (Cullis et al., 1997; Rosilio, 2017). As seen in Figure 2, at higher surface pressures ( $\pi \geq 28$  mN/m), the molecular area decreases more significantly, indicating stronger molecular condensation and increased monolayer stability. A significant pH-dependent effect is observed, where  $A_{12}$  values at pH 4.8 are consistently higher than at pH 7.4. This suggests that acidic conditions weaken lipid-lipid interactions, leading to more expanded monolayers, whereas neutral pH promotes stronger Chol-lipid interactions, resulting in denser packing. Additionally, Figure 2 illustrates that higher surface pressures result in stronger molecular condensation, confirming that Chol stabilizes the monolayer by increasing its resistance to compression (Moya Betancourt et al., 2023; Szcześ et al., 2012). Since MNPs are present in all conditions, their effect on molecular areas must be considered alongside Chol and pH effects. The data suggest that at low  $x_{\text{Chol}}$ ,  $A_{12}$  values remain larger due to steric hindrance induced by MNPs (Oliveira et al., 2022; Piosik et al., 2021). However, at  $x_{\text{Chol}} \geq 0.5$ , Chol overcomes this effect, promoting lipid packing despite the presence of nanoparticles. The observation that  $\pi$  values decrease with increasing  $x_{\text{Chol}}$  further supports the idea that Chol modulates the interaction between monolayer components, altering the packing density and fluidity of the monolayer. These findings confirm that Chol enhances lipid condensation up to  $x_{\text{Chol}} \approx 0.5$ , particularly at higher  $\pi$  values and pH 7.4, whereas at pH 4.8, the monolayer remains slightly expanded, reflecting weaker lipid cohesion.

### 3.3. Deviations from Ideal Mixing: Excess Molecular Area Analysis

The  $A_{\text{exc}}$  provides a more detailed understanding of whether Chol and DPPC form an ideal or non-ideal mixture in the presence of MNPs. Negative  $A_{\text{exc}}$  values indicate that the system favors condensation (strong lipid-Chol interactions), whereas positive values suggest molecular expansion (weaker lipid interactions or phase separation tendencies) (Figure 3). The  $A_{\text{exc}}$  values were calculated using equation 3), where  $A_{12}^{\text{real}}$  represents the experimentally determined molecular area, while  $A_{12}^{\text{ideal}}$  is obtained assuming ideal mixing based on equation 4). As shown in Figure 3, at low  $x_{\text{Chol}}$  ( $\leq 0.25$ ),  $A_{\text{exc}}$  values remain close to zero or slightly positive, suggesting that Chol initially integrates into the DPPC monolayer with minimal disruption. However, as  $x_{\text{Chol}}$  increases toward 0.25-0.50,  $A_{\text{exc}}$  becomes more negative ( $\sim -6$  to  $-8$   $\text{\AA}^2/\text{molecule}$  at pH 7.4), indicating that Chol promotes molecular condensation and enhances lipid-lipid interactions (Moya Betancourt et al., 2023; Szcześ et al., 2012). Figure 3(a) illustrates that at pH 4.8, weaker electrostatic interactions result in less pronounced

condensation effects, while Figure 3(b) confirms that at pH 7.4,  $A_{\text{exc}}$  reaches its most negative values, suggesting stronger Chol-DPPC interactions (Ding et al., 2016; Gong et al., 2002).

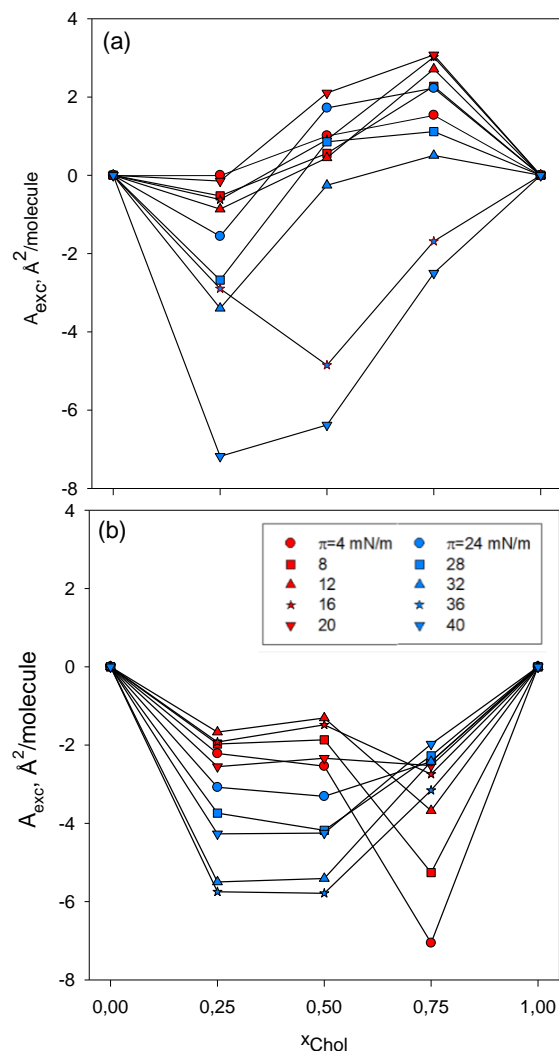


**Figure 3.**  $A_{\text{exc}}-x_{\text{Chol}}$  curves obtained at different surface pressures for Chol/DPPC-MNP monolayers at (a) pH=4.8 and (b) pH=7.4.

A strong pH-dependent effect is evident, where  $A_{\text{exc}}$  values at pH 7.4 reach more negative values compared to pH 4.8. This suggests that neutral pH facilitates stronger Chol-DPPC interactions, favoring more efficient molecular packing, while at pH 4.8, weaker electrostatic interactions between lipid headgroups lead to a less pronounced condensation effect. The most negative  $A_{\text{exc}}$  values, indicating the highest molecular attraction and optimal lipid condensation, were observed at  $x_{\text{Chol}} = 0.25$  for pH 4.8 and  $x_{\text{Chol}} = 0.50$  for pH 7.4, as seen in Figure 3. These compositions represent the most thermodynamically stable conditions for each pH level (Jurak et al., 2018). At pH 4.8, the most negative  $A_{\text{exc}}$  value is observed at  $x_{\text{Chol}} = 0.25$ , while at pH 7.4, it occurs at  $x_{\text{Chol}} = 0.50$ . This difference arises because at pH 4.8, the increased protonation of DPPC headgroups weakens electrostatic attraction, making lower Chol

concentrations ( $x_{\text{Chol}}=0.25$ ) more favorable for lipid condensation. Conversely, at pH 7.4, reduced protonation allows Chol to integrate more effectively into the monolayer, leading to maximum condensation at  $x_{\text{Chol}} = 0.50$ . Although  $x_{\text{Chol}}=0.75$  contains a higher Chol fraction,  $A_{\text{exc}}$  begins to increase again at this concentration, suggesting that excessive Chol disrupts uniform lipid packing and induces steric hindrance effects rather than further enhancing molecular condensation. These conditions correspond to the most efficient molecular packing, strongest lipid-Chol interactions, and the most thermodynamically stable monolayer structures. Since MNPs were present in all experimental conditions, their impact on non-ideal mixing must be considered. The presence of MNPs slightly increases  $A_{\text{exc}}$  values at low  $x_{\text{Chol}}$ , suggesting that nanoparticle-lipid interactions introduce steric constraints that counteract Chol condensation effect. However, at  $x_{\text{Chol}}\approx 0.25-0.50$ , the stabilizing effect of Chol dominates, leading to the most negative  $A_{\text{exc}}$  values, confirming that this composition represents the optimal Chol-DPPC interaction state. These results confirm that Chol enhances lipid condensation up to  $x_{\text{Chol}}\approx 0.50$ , particularly at pH 7.4, while higher  $x_{\text{Chol}}$  levels lead to steric effects and phase separation tendencies. The data also highlights a competitive relationship between Chol and MNPs, where Chol stabilizes lipid packing and reduces nanoparticle-induced perturbations. The interpretation of  $A_{\text{exc}}$  values further supports that when  $A_{\text{exc}}$  is positive (experimental values  $>$  theoretical values), the system is not fully miscible, and repulsive intermolecular forces dominate. Conversely, when  $A_{\text{exc}}$  is negative (experimental values  $<$  theoretical values), the system is fully miscible, and attractive intermolecular forces dominate (He et al., 2014; Jurak et al., 2018). The most negative  $A_{\text{exc}}$  values indicate the strongest intermolecular attraction, leading to the highest molecular packing efficiency. Thus, the system reaches its highest molecular attraction, miscibility, and packing efficiency when  $A_{\text{exc}}$  reaches its most negative values: at  $x_{\text{Chol}}=0.25$  for pH 4.8 and  $x_{\text{Chol}}=0.50$  for pH 7.4. Under these conditions, the system exhibits the strongest lipid-Chol interactions, optimal lipid condensation, and the most thermodynamically stable monolayer structure.

### 3.4. Thermodynamic Stability: Excess Gibbs Free Energy of Mixing Analysis

The  $\Delta G_{\text{exc}}$  of mixing provides insights into the thermodynamic stability of Chol/DPPC monolayers in the presence of MNPs. By evaluating deviations from ideal mixing,  $\Delta G_{\text{exc}}$  helps determine whether the system exhibits homogeneous mixing, enhanced lipid-lipid interactions, or phase separation tendencies. A negative  $\Delta G_{\text{exc}}$  value indicates thermodynamically favorable lipid mixing and strong molecular interactions, whereas positive values suggest phase separation or repulsive interactions between the components. The  $\Delta G_{\text{exc}}$  values were determined using equation 5) and analyzed under different surface pressures and pH conditions. As shown

in Figure 4, at low  $x_{\text{Chol}} (\leq 0.25)$ ,  $\Delta G_{\text{exc}}$  values are close to zero or slightly negative, suggesting that Chol initially integrates into the DPPC monolayer without significantly altering its thermodynamic stability. However, as  $x_{\text{Chol}}$  increases toward 0.50,  $\Delta G_{\text{exc}}$  reaches its most negative value ( $\sim -750$  J/mol at pH 4.8 and  $\sim -900$  J/mol at pH 7.4), confirming that Chol enhances lipid-lipid interactions and promotes thermodynamically favorable mixing at this composition (Moya Betancourt et al., 2023; Szcześ et al., 2012). Figure 4(a) illustrates that at pH 4.8, weaker electrostatic interactions result in reduced thermodynamic stability, while Figure 4(b) confirms that at pH 7.4,  $\Delta G_{\text{exc}}$  reaches its most negative values, suggesting stronger Chol-DPPC interactions (Ding et al., 2016; Gong et al., 2002).

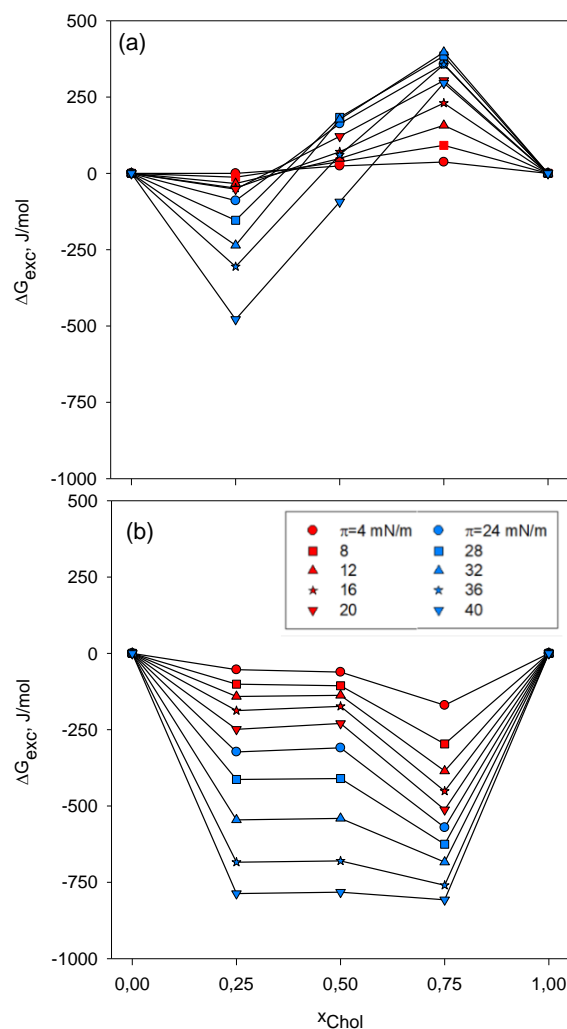


**Figure 4.**  $\Delta G_{\text{exc}}-x_{\text{Chol}}$  curves obtained at different surface pressures for Chol/DPPC-MNP monolayers at (a) pH=4.8 and (b) pH=7.4.

The effect of pH is significant, as  $\Delta G_{\text{exc}}$  values are consistently lower at pH 7.4 compared to pH 4.8, indicating that Chol incorporation into the monolayer is more thermodynamically stable at neutral pH. This trend supports the hypothesis that reduced electrostatic repulsion at pH 7.4 enhances lipid-Chol interactions,

increasing monolayer stability. At pH 4.8,  $\Delta G_{exc}$  values are less negative, suggesting that protonation of DPPC headgroups weakens Chol-induced stabilization, resulting in reduced lipid miscibility and a higher tendency for phase separation. As seen in Figure 4, at  $x_{Chol} \geq 0.50$ ,  $\Delta G_{exc}$  values increase toward zero, and at  $x_{Chol} = 1.0$ ,  $\Delta G_{exc}$  becomes slightly positive ( $\sim +50$  to  $+150$  J/mol at pH 4.8), indicating that excess Chol disrupts monolayer homogeneity, leading to steric hindrance and phase separation tendencies (Oliveira et al., 2022; Piosik et al., 2021). These findings suggest competitive interaction between Chol and MNPs, where Chol enhances monolayer stability by promoting lipid ordering and reducing nanoparticle-induced disruptions. However, at high  $x_{Chol}$ , steric effects and phase separation tendencies begin to dominate, reducing thermodynamic stability. The results confirm that Chol concentration and pH are key regulators of monolayer stability, influencing lipid-lipid interactions, nanoparticle incorporation, and phase behavior.  $\Delta G_{exc}$  is an important indicator of monolayer miscibility and stability. When  $\Delta G_{exc} = 0$ , the system behaves ideally, meaning that molecular interactions are balanced, and the components are completely miscible. If  $\Delta G_{exc}$  is negative, attractive forces dominate, leading to a more stable and condensed monolayer. Conversely, if  $\Delta G_{exc}$  is positive, repulsive interactions become dominant, increasing the likelihood of phase separation (Szcześ et al., 2012; He et al., 2014; Jurak et al., 2018; Vázquez-González et al., 2019). At pH 4.8, the most negative  $\Delta G_{exc}$  value occurs at  $x_{Chol}=0.25$ , confirming that at this composition, attractive forces dominate, and the monolayer is at its most thermodynamically stable state. Similarly, at pH 7.4, the most negative  $\Delta G_{exc}$  value is observed at  $x_{Chol}=0.50$ , indicating that this composition provides the optimal balance between lipid-Chol interactions and monolayer stabilization. These findings agree with the  $A_{exc}$  analysis, where the strongest molecular interactions were also observed at  $x_{Chol}=0.25$  for pH 4.8 and  $x_{Chol}=0.50$  for pH 7.4. The negative  $\Delta G_{exc}$  values further confirm that attractive forces (adhesion) are dominant in these conditions, supporting the hypothesis that Chol enhances lipid packing and monolayer integrity (Oliveira et al., 2022). Although pH 7.4 shows entirely negative  $\Delta G_{exc}$  values across all compositions, indicating that attractive interactions are dominant at all Chol concentrations, pH 4.8 exhibits negative  $\Delta G_{exc}$  values only at  $x_{Chol}=0.25$ , while other compositions tend toward zero or positive values, signifying the increasing role of repulsive forces. This demonstrates that lipid miscibility and monolayer stability are strongly pH-dependent, with pH 7.4 providing overall greater thermodynamic stability.

### 3.5. Monolayer Elasticity: Compressibility Modulus Analysis

The  $C_s^{-1}$  is a critical parameter that reflects the mechanical stability and elasticity of lipid monolayers, providing insights into how Chol and MNPs influence lipid packing under compression. Higher  $C_s^{-1}$  values

indicate greater monolayer rigidity and stronger molecular interactions, whereas lower values suggest a more fluid and disordered system. The  $C_s^{-1}$  values were analyzed under different surface pressures, pH conditions (4.8 and 7.4), and  $x_{Chol}$  compositions (0, 0.25, 0.50, 0.75, and 1.0) to evaluate their impact on monolayer mechanics (Figure 5). The values were determined using equation 6). As shown in Figure 5,  $C_s^{-1}$  increases with  $x_{Chol}$ , confirming that Chol enhances monolayer rigidity by promoting lipid ordering and reducing molecular free volume. At  $x_{Chol} \leq 0.25$ ,  $C_s^{-1}$  remains relatively low ( $\sim 80$ - $100$  mN/m), reflecting a more fluid monolayer with greater molecular disorder. However, as  $x_{Chol}$  increases,  $C_s^{-1}$  rises significantly, reaching  $\sim 90$ - $100$  mN/m at  $x_{Chol} \approx 0.50$ - $0.75$ , suggesting that Chol promotes tighter molecular packing and enhances monolayer stiffness (Szcześ et al., 2012; Moya Betancourt et al., 2023). At  $x_{Chol}=1.0$ ,  $C_s^{-1}$  slightly decreases ( $\sim 70$ - $80$  mN/m), indicating that excessive Chol may lead to lateral phase separation and reduce monolayer homogeneity.

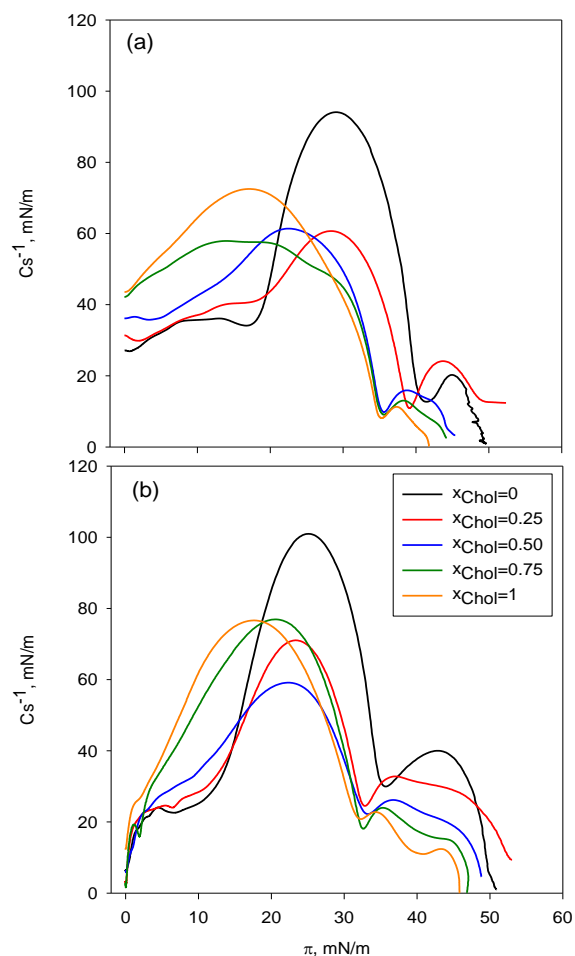


**Figure 5.**  $C_s^{-1}$ - $\pi$  curves obtained at different composition ratios of Chol/DPPC-MNP at (a) pH=4.8 and (b) pH=7.4.

The pH effect is also evident, as monolayers at pH 7.4 exhibit consistently higher  $C_s^{-1}$  values than those at pH 4.8. At neutral pH, stronger lipid-lipid and Chol-DPPC interactions enhance monolayer stability, leading to

higher  $C_s^{-1}$  values. In contrast, at pH 4.8,  $C_s^{-1}$  values (~15-30% lower than at pH 7.4) indicate increased molecular disorder and reduced lipid packing efficiency, likely due to weaker electrostatic interactions among protonated DPPC headgroups. The realistic lateral pressure range for cell membranes (30-35 mN/m) shows that  $C_s^{-1}$  decreases with increasing  $x_{\text{Chol}}$ , indicating that higher Chol concentrations or reduced DPPC content led to a more compressible monolayer. This is expected, as DPPC has a denser structure compared to Chol, contributing to greater monolayer rigidity at lower  $x_{\text{Chol}}$  values (Marsh, 1996; Torrano et al., 2013; Jurak et al., 2018; Oliveira et al., 2022). These findings agree with Jurak (2013), who demonstrated that cholesterol enhances lipid ordering and reduces molecular free volume, increasing monolayer stiffness at moderate concentrations. At pH 4.8, the highest  $C_s^{-1}$  values are observed at  $x_{\text{Chol}}=0.25$ , indicating that at this composition, the monolayer reaches maximum rigidity under acidic conditions. However, at pH 7.4,  $C_s^{-1}$  is highest at  $x_{\text{Chol}}=0.50$ , confirming that this composition provides optimal lipid packing stability at neutral pH. These findings are consistent with Jurak (2013), who reported that at intermediate cholesterol levels, lipid condensation and molecular packing efficiency are maximized. Furthermore, this trend aligns with thermodynamic stability results from the  $A_{\text{exc}}$  and  $\Delta G_{\text{exc}}$  analyses, where the strongest molecular interactions were observed at  $x_{\text{Chol}}=0.25$  for pH 4.8 and  $x_{\text{Chol}}=0.50$  for pH 7.4. The agreement between compressibility modulus and thermodynamic stability trends further confirms that cholesterol plays a key role in regulating lipid monolayer mechanics. At high  $x_{\text{Chol}}$  values ( $\geq 0.75$ ),  $C_s^{-1}$  slightly decreases, which suggests steric hindrance and potential lipid domain formation at excessive Chol concentrations. This is consistent with previous studies indicating that high cholesterol levels can lead to lateral phase separation, where Chol-enriched domains disrupt uniform lipid packing, reducing monolayer stiffness (Jurak, 2013). This trend is further supported by  $\Delta G_{\text{exc}}$  results, where the system shows reduced thermodynamic stability at high  $x_{\text{Chol}}$  due to steric effects and phase segregation. Since MNPs were incorporated in all experiments, their influence must be evaluated in conjunction with Chol and pH effects. As illustrated in Figure 5, at low  $x_{\text{Chol}}$ , MNP-induced structural disruptions reduce  $C_s^{-1}$  values. However, at  $x_{\text{Chol}} \approx 0.50$ , the stabilizing effect of Chol dominates, maintaining high  $C_s^{-1}$  values and counteracting the destabilizing influence of MNPs (Szcześ et al., 2012; Moya Betancourt et al., 2023). These results confirm that Chol and pH are key regulators of monolayer mechanical properties, with Chol enhancing monolayer elasticity at intermediate  $x_{\text{Chol}}$  values and pH 7.4 providing additional stabilization. The interplay between lipid-lipid interactions, nanoparticle incorporation, and Chol concentration ultimately determines monolayer rigidity, influencing the overall mechanical behavior of biomimetic membranes.

#### 4. Conclusion

This study investigated the phase behavior, molecular organization, and thermodynamic properties of Chol/DPPC monolayers incorporating hydrophobic MNPs under varying  $x_{\text{Chol}}$  and pH conditions (4.8 and 7.4), providing critical insights into how these factors influence lipid monolayer stability, molecular packing, and mechanical properties. The  $\pi$ -A isotherm analysis confirmed that Chol enhances monolayer condensation up to  $x_{\text{Chol}} \approx 0.50$ , particularly at higher surface pressures and pH 7.4, whereas pH 4.8 resulted in more expanded monolayers due to weaker lipid-lipid interactions. The  $A_{12-x_{\text{Chol}}}$  analysis demonstrated that Chol reduces molecular area in a non-linear manner, with the most pronounced condensation effect observed at intermediate  $x_{\text{Chol}}$  values, beyond which steric hindrance and phase separation tendencies emerged. The  $A_{\text{exc}}$  analysis revealed deviations from ideal mixing, where negative  $A_{\text{exc}}$  values at  $x_{\text{Chol}}=0.25$  (pH 4.8) and  $x_{\text{Chol}}=0.50$  (pH 7.4) indicated strong Chol-lipid interactions and optimal lipid condensation, while higher  $x_{\text{Chol}}$  values led to steric constraints and non-ideal mixing effects. The excess  $\Delta G_{\text{exc}}$  of mixing analysis confirmed that Chol enhances monolayer thermodynamic stability up to  $x_{\text{Chol}}=0.50$  at pH 7.4, whereas at pH 4.8,  $x_{\text{Chol}}=0.25$  represented the most stable composition, after which phase separation effects and steric hindrance from excess Chol molecules became dominant. The  $C_s^{-1}$  analysis demonstrated that Chol increases monolayer rigidity, with higher  $C_s^{-1}$  values at pH 7.4 indicating a mechanically more stable monolayer, while at high  $x_{\text{Chol}}$  ( $\geq 0.75$ ),  $C_s^{-1}$  slightly decreased, suggesting steric hindrance and lateral phase separation effects. The presence of MNPs resulted in increased molecular area and slightly reduced  $C_s^{-1}$  values at low  $x_{\text{Chol}}$ , indicating steric effects that disrupted lipid packing; however, at  $x_{\text{Chol}} \geq 0.50$ , Chol stabilizing role counteracted these nanoparticle-induced perturbations, maintaining monolayer integrity and rigidity. These findings confirm that Chol regulates lipid packing, phase transitions, and thermodynamic stability, while pH influences lipid-lipid interactions and MNPs introduce steric modifications to the monolayer structure, demonstrating the strong correlation between  $C_s^{-1}$ ,  $A_{\text{exc}}$ , and  $\Delta G_{\text{exc}}$  trends. Understanding these interactions is essential for designing biomimetic membranes, lipid-nanoparticle systems, and nanostructured lipid platforms in biomedical and nanotechnological applications, while future studies should focus on real-time lipid-nanoparticle interactions and their impact on monolayer stability under dynamic conditions.

**Author Contributions**

The percentages of the authors' contributions are presented below. All authors reviewed and approved the final version of the manuscript.

	N.S.	S.S.	U.S.
C	40	30	30
D	40	30	30
S	40	30	30
DCP	40	30	30
DAI	40	30	30
L	40	30	30
W	40	30	30
CR	40	30	30
SR	40	30	30
PM	40	30	30
FA	40	30	30

C=Concept, D= design, S= supervision, DCP= data collection and/or processing, DAI= data analysis and/or interpretation, L= literature search, W= writing, CR= critical review, SR= submission and revision, PM= project management, FA= funding acquisition.

**Conflict of Interest**

The authors declared that there is no conflict of interest.

**Ethical Consideration**

Ethics committee approval was not required for this study because of there was no study on animals or humans.

**References**

Bodik M, Jergel M, Majkova E, Siffalovic P. 2020. Langmuir films of low-dimensional nanomaterials. *Adv Colloid Interface Sci*, 283: 102239.

Cullis PR, Hope MJ, Bally MB, Madden TD, Mayer LD, Fenske DB. 1997. Influence of pH gradients on the transbilayer transport of drugs, lipids, peptides, and metal ions into large unilamellar vesicles. *Biochim Biophys Acta*, 1331: 187-211.

Dana RM. 1999. The monolayer technique: a potent tool for studying the interfacial properties of antimicrobial and membrane-lytic peptides and their interactions with lipid membranes. *Biochim Biophys Acta*, 1462: 109-140.

Ding C, Tong L, Feng J, Fu J. 2016. Recent advances in stimuli-responsive release function drug delivery systems for tumor treatment. *Molecules*, 21: 1715.

Ganta S, Devalapally H, Shahiwala A, Amiji M. 2008. A review of stimuli-responsive nanocarriers for drug and gene delivery. *J Control Release*, 126(3): 187-204.

Gao W, Chan JM, Farokhzad OC. 2010. pH-responsive nanoparticles for drug delivery. *Mol Pharm*, 7(6): 1913-20.

Gong K, Feng SS, Go ML, Soew PH. 2002. Effects of pH on the stability and compressibility of DPPC/cholesterol monolayers at the air-water interface. *Colloids Surf. A: Physicochem. Eng Asp*, 207: 113-125.

Hao C, Li J, Mu W, Zhu L, Yang J, Liu T, Li B, Chen S, Sun R. 2016. Adsorption behavior of magnetite nanoparticles into the DPPC model membranes. *Appl Surf Sci*, 362: 121-125.

He H, Sun R, Hao C, Yang J, Wang M, Zhang L. 2014. Thermodynamic analysis and AFM study of the interaction

of palmitic acid with DPPE in Langmuir monolayers. *Colloids Surf. A: Physicochem Eng Asp*, 441: 184-194.

Jurak M. 2013. Thermodynamic aspects of cholesterol effect on properties of phospholipid monolayers: Langmuir and Langmuir-Blodgett monolayer study. *J Phys Chem B*, 117(12): 3496-3502.

Jurak M, Mroczka R, Łopucki R. 2018. Properties of artificial phospholipid membranes containing lauryl gallate or cholesterol. *J Membr Biol*, 251: 277-294.

Marsh D. 1996. Lateral pressure in membranes. *Biochim. Biophys Acta*, 1286: 183-223.

Moya Betancourt SN, Cámara CI, Riva JS. 2023. Interaction between pharmaceutical drugs and polymer-coated Fe3O4 magnetic nanoparticles with Langmuir monolayers as cellular membrane models. *Pharmaceutics*, 15: 311.

Oliveira ON Jr, Caseli L, Ariga K. 2022. The past and the future of Langmuir and Langmuir-Blodgett films. *Chem Rev*, 122: 6459-6513.

Peetla C, Jin S, Weimer J, Elegbede A, Labhasetwar V. 2014. Biomechanics and thermodynamics of nanoparticle interactions with plasma and endosomal membrane lipids in cellular uptake and endosomal escape. *Langmuir*, 30: 7522-7532.

Piosik E, Ziegler-Borowska M, Chełminiak-Dudkiewicz D, Martyński T. 2021. Effect of aminated chitosan-coated Fe3O4 nanoparticles with applicational potential in nanomedicine on DPPG, DSPC, and POPC Langmuir monolayers as cell membrane models. *Int J Mol Sci*, 22: 2467.

Rosilio V. 2017. How can artificial lipid models mimic the complexity of molecule-membrane interactions? *Adv. Biomembr. Lipid Self-Assembly*, 27: 107-141.

Salas SD, Villanueva ME, Selzer SM, Ferreyra NF, Vico RV. 2024. A systematic study of the impact of aromatic/aliphatic amines and protein corona as coatings of iron oxide magnetic nanoparticles on the interaction with DPPC Langmuir monolayers. *Surf Interfaces*, 51: 104771.

Swierczewski M, Bürgi T. 2023. Langmuir and Langmuir-Blodgett films of gold and silver nanoparticles. *Langmuir*, 39: 2135-2151.

Szczeń A, Jurak M, Chibowski E. 2012. Stability of binary model membranes—Prediction of the liposome stability by the Langmuir monolayer study. *J Colloid Interface Sci*, 372: 212-216.

Torrano AA, Pereira ÂS, Oliveira Jr ON, Barros-Timmons A. 2013. Probing the interaction of oppositely charged gold nanoparticles with DPPG and DPPC Langmuir monolayers as cell membrane models. *Colloids Surf B: Biointerfaces*, 108: 120-126.

Vázquez-González ML, Botet-Carreras A, Domènech Ò, Montero TM, Borrell JH. 2019. Planar lipid bilayers formed from thermodynamically-optimized liposomes as new featured carriers for drug delivery systems through human skin. *Int J Pharm*, 563: 1-8.

Wrobel EC, Guimarães IDL, Wohnrath K, Oliveira ON Jr. 2024. Effects induced by η<sup>6</sup>-p-cymene ruthenium(II) complexes on Langmuir monolayers mimicking cancer and healthy cell membranes do not correlate with their toxicity. *Biochim Biophys Acta Biomembr*, 1866: 184332.

Zhang W, Wang F, Wang Y, Wang J, Yu Y, Guo S, Chen R, Zhou D. 2016. pH and near-infrared light dual-stimuli responsive drug delivery using DNA-conjugated gold nanorods for effective treatment of multidrug resistant cancer cells. *J Control Release*, 82: 204.